Angewandte Chemie
Eine Zeitschrift der Gesellschaft Deutscher Chemiker

Supporting Information

69451 Weinheim, Germany

A New Mechanistic Probe for Transition Metal-Mediated O_2 Activation

*Michael P. Lanci, David W. Brinkley, Kristie L. Stone, Valeriy V. Smirnov, Justine P. Roth**

Department of Chemistry, The Johns Hopkins University,

3400 N. Charles Street, Baltimore, MD 21218

E-mail: jproth@jhu.edu

General Experimental:

All manipulations employed standard high vacuum techniques or a N_2-filled glove box. Manometry was performed using vacuum apparatus equipped with a capacitance manometer. The measurements were performed in concert with preparation of samples for isotope effect determination; i.e. O_2 was present in >10-fold excess over the reduced metal compound. Specialty chemicals were obtained from Aldrich unless noted. 'Anhydrous' *N*,*N*-dimethylformamide (DMF) and dimethylsulfoxide (DMSO) were obtained from Burdick and Jackson and used as received. Other solvents obtained commercially were purified according to standard protocols.[1] Deuterated solvents were obtained from Cambridge Isotope Laboratories and stored protected from light at -30 °C. NMR experiments were performed on Brüker Avance 300 and 400 MHz spectrometers. Samples containing reduced metal compounds (1-4.5 mM) were typically reacted by saturating both the solution and atmosphere above the solution with 1 atm O_2. ^{1}H shifts are reported in parts per million relative to residual protio solvent. ^{31}P shifts are reported relative to 85% Phosphoric Acid-d_3. Hexamethyldisiloxane and tetra-*n*-butylammonium hexafluorophosphate were used as internal standards. Electronic absorbance spectra were obtained on an Agilent 8453 UV-visible spectrophotometer. Stopped-flow UV-vis experiments were performed on an OLIS RSM1000. Infrared spectra were obtained using a Brüker Equinox 55. Electrospray mass spectral data were collected using a ThermoQuest Finnigan LCQ_{DECA} LC/MS. Elemental analysis was performed by Desert Analytics Inc. (Tucson, AZ). Isotope ratio analysis of CO_2 samples was performed using a Micromass Isoprime stable isotope mass spectrometer equipped with dual-inlet system (Johns Hopkins University Department of Earth and Planetary Sciences).

Determination of Reaction Yields:

Vaska's complex, *trans*-$Ir(PPh_3)_2(CO)Cl$ (**Ir**), was prepared following a published procedure[2] and recrystallized from toluene. Purity was confirmed by: $\{^1H\}^{31}P$ NMR (**Ir**: δ 25.6 DMF-d_7, δ 24.8 DMSO-d_6), elemental analysis: *calc*: 56.96 %C, 3.88 %H; *found*: 56.78 %C,

3.82 %H and comparison with the published extinction coefficients.[3-5] Exposure of **Ir** to an atmosphere of O_2 gave $IrO_2Cl(PPh_3)_2(CO)$ (**IrO_2**) as indicated by a single peak in the ^{31}P NMR spectrum (δ 3.41 DMF-d_7, δ 4.22 DMSO-d_6).[4] Yields of 92 ± 7 % (DMF) and 99 ±_7 % (DMSO) were confirmed using the extinction coefficients for **Ir** and **IrO_2** (ε_{386} = 240 ± 20 $M^{-1}cm^{-1}$ (DMF) and ε_{386nm} = 160 ± 40 $M^{-1}cm^{-1}$ (DMSO). The latter were determined using an analytically pure sample of **IrO_2**: *calc:* 54.71 %C, 3.72 %H; *found:* 54.23 %C, 3.78 %H. Manometry measurements indicated that the ratio of O_2 consumed per equivalent of **Ir** was (1 ± 0.1):1 and independent of solvent.

$[Ir(dppe)_2]Cl$; dppe = 1,2 bis(diphenylphosphino)ethane (**Ir_{dppe}**) was prepared according to a published procedure.[6] Recrystallization from acetonitrile/Et_2O afforded orange crystals. Purity was confirmed by ^1H (δ 7.38 8H, δ 7.28 32H; δ 2.18, 8H) and $\{^1H\}^{31}P$ NMR (**Ir_{dppe}**: δ 50.86 DMSO-d_6), elemental analysis: *calc:* 60.96 %C, 4.72 %H; *found:* 61.32 %C, 4.50 %H and comparison with the published extinction coefficients.[7] Oxygenation in DMSO-d_6 gave $[IrO_2(dppe)_2]Cl$ (**$Ir_{dppe}O_2$**) by $\{^1H\}^{31}P$ NMR (δ 15.4, δ 19.5) in a yield of 97 ± 5%. The ratio of O_2 consumed per equivalent of **Ir_{dppe}** was determined by manometry to be (1 ± 0.05):1 in DMF and DMSO.

Tetrakis(triphenylphosphine)platinum(0) (**Pt**) was prepared following a published procedure.[8] Recrystallization from acetone afforded $Pt(PPh_3)_4$ *calc:* 69.50 %C, 4.86 %H; *found:* 69.26 %C, 4.93 %H. The $\{^1H\}^{31}P$ NMR spectrum at -80 °C in toluene-d_8 indicated an equilibrium mixture of $Pt(PPh_3)_4$ (δ 10.6, J_{Pt-P} = 3833 Hz) and $Pt(PPh_3)_3$ (δ 51.2, J_{Pt-P} = 4468 Hz) as previously reported.[9] At ambient temperature, the $\{^1H\}^{31}P$ NMR spectrum is irresolvably broadened due to rapid ligand exchange. Spectrophotometric titration in benzene and DMF confirmed that **Pt** is largely dissociated to $Pt(PPh_3)_3$ {ε_{440} = 620 $M^{-1}cm^{-}1$} in the presence of excess PPh_3 (≤ 0.2 M).[10]

$\{^1H\}^{31}P$ NMR analysis of the reaction between **Pt** and excess O_2 in DMF-d_7 at -45 ^oC indicated initial formation of $PtO_2(PPh_3)_2$ (**PtO_2**) (δ16.9, J_{Pt-P} = 4049) and two equivalents of free PPh_3 (δ -4.96). Upon warming the solution to ambient temperature, $(O)PPh_3$ (δ 25.9) formed in

84 ± 20% yield based on $[\mathbf{Pt}]_{initial}$. Over the same time period the yield of $\mathbf{PtO_2}$ was 107 ± 7%. Manometry measurements indicated 1.6 ± 0.4 moles of O_2 consumed per mole of **Pt**. The yield is consistent with a previously proposed mechanism involving protonolysis of $\mathbf{PtO_2}$ by residual water and oxidation of PPh_3 by H_2O_2 as well as by a "$Pt^{II}(O)$" intermediate.[11]

Tetrakis(triphenylphosphine)palladium(0) (**Pd**) was purchased from Strem Chemicals and analyzed for purity by elemental analysis: *calc:* 74.84 %C, 5.23 %H; *found:* 75.08 %C, 5.43 %H. Previous studies have shown that **Pd** is largely dissociated in solution to $Pd(PPh_3)_3$, $Pd(PPh_3)_2$ and free PPh_3.[12, 13] The $^{31}P\{^1H\}$ NMR spectrum at ambient temperature in DMF-d_7 exhibits a single broad resonance at δ 17.1.

Reaction of a DMF solution prepared from **Pd** with excess O_2 gave $\mathbf{PdO_2}$ in 100 ± 16 % yield as indicated by $\{^1H\}^{31}P$ NMR: δ 34.3.[14] Free PPh_3 (76 ± 18 %) and $PPh_3(O)$ (24 ± 18 %) were also produced, the latter based on $[\mathbf{Pd}]_{initial}$. Consistent with the formation of a stable $\mathbf{PdO_2}$, manometry measurements indicated 1.2 ± 0.2 moles of O_2 consumed per mole of **Pd**.

Tetrakis(triphenylphosphine)nickel(0) (**Ni**) was isolated as a dark red solid following a published procedure.[15] Purity was confirmed by elemental analysis: *calc:* 78.06 %C, 5.46 %H; *found:* 78.00 %C, 5.60 %H. $\{^1H\}^{31}P$ NMR gave disparate results depending on the solvent. DMF-d_7 solutions appeared dark red and exhibited a single broad resonance at δ 22.26 which integrated to four phosphorus ligands. Upon cooling to -60 °C, the signal sharpened and shifted downfield to δ 25.85 and a broad peak corresponding to PPh_3 appeared at δ -7.56. The signals integrated to 85% ± 23% and 16% ± 8%, respectively, consistent with exchange between $Ni(PPh_3)_3$ and free PPh_3. Previous studies in toluene-d_8 reported rapid exchange between $Ni(PPh_3)_3$ and free PPh_3 at room temperature and formation of $Ni(PPh_3)_4$ δ 24.1ppm at -80 ºC.[16] DMSO-d_6 solutions of **Ni** appeared yellow-green and two signals were observed in a 1:1 ratio at δ 25.41 (23.5 Hz) and δ -5.62 (98.5Hz). The former corresponded to two equivalents of PPh_3 bound to Ni^0 and the latter to two equivalents of free PPh_3. Electrospray mass spectral measurements indicated the presence of $Ni(PPh_3)_2(DMSO)$(659.69 m/Z) as well as small amount of $Ni(PPh_3)_3$ (843.34 m/Z).

Exposure of solutions prepared from **Ni** to excess O_2 resulted in rapid loss of color and formation of free PPh_3 and $(O)PPh_3$ as the only phosphorus-containing products. Transient signals, possibly corresponding to **NiO_2** and some variant were observed at δ 36.0 ppm and δ 29.0 ppm at -40 °C in DMF. Upon warming this solution to ambient temperature, the yields of PPh_3 and $PPh_3(O)$ were 70 ± 18% and 108 ± 26%, respectively, based on **Ni.** Manometry measurements indicated 2.3 ± 0.8 moles of O_2 were consumed per mole of **Ni**. In DMSO, PPh_3 and $PPh_3(O)$ were obtained in 118 ± 20 % and 82 ± 20 % yields, respectively, based on **Ni.** The ^1H NMR revealed a broad signal at 3.22 consistent with the formation of a Ni^{II} solvento species.[17, 18] Manometry measurements indicated 1.2 ± 0.2 moles of O_2 were consumed per mole of **Ni**.

Tetrakis(tert-butylisocyanide)nickel(0) (**Ni_{isc}**) was prepared following a published procedure [19]. Recrystallization from toluene at -30 °C afforded large gold crystals. NMR and elemental analysis indicated the composition $Ni(CN^tBu)_4$•0.5 toluene: *calc:* 64.55 %C, 9.22 %H, 12.81 %N; *found:* 64.78 %C, 9.50 %H, 12.56 %N. Earlier cryoscopic studies indicated dissociation of **Ni_{isc}** to $Ni(CN^tBu)_3$.[20] ^1H NMR spectra of solutions prepared from **Ni_{isc}** exhibit a single peak (δ 1.36 in DMF-d_7 and δ 1.13 in toluene-d_8) which integrates to 36 protons. At -50 °C in DMF-d_7, the signal shifts to δ 1.28 but no sign of decoalescence is detected. Addition of CN^tBu, gives a new broad signal at δ 1.40 which coalesces with the signal at δ 1.28 and shifts to δ 1.36 upon warming the sample to room temperature. The results are consistent with multiple Ni^0-species undergoing rapid ligand exchange on the NMR time scale.

Reaction with excess O_2 in DMF-d_7 at ambient temperature reveals a new resonance due to $NiO_2(CN^tBu)_2$ (**$Ni_{isc}O_2$**) (δ 1.47) integrating to 36 protons. This signal apparently corresponds to a weighted average of free CN^tBu and **$Ni_{isc}O_2$** yet cooling the sample to -50 °C does not result in decoalescence. A yield of 103 ± 10% **$Ni_{isc}O_2$** was confirmed by UV-vis spectrophotometry using published extinction coefficients.[19.] On an NMR scale, **$Ni_{isc}O_2$** decomposed gradually over the course of twelve hours affording OCN^tBu and a new signal at δ1.25.

The infrared spectrum of **Ni_{isc}** in DMF is characterized by a single, broad C–N stretch at 2020 cm-1. Monitoring the oxygenation revealed three sharp stretches at 2198, 2172 and 2136 cm^{-1}. The first two frequencies correspond to the asymmetric and symmetric C–N modes of **$Ni_{isc}O_2$** and the third to free CN^tBu. A stretch at 907 cm^{-1} is also observed in good agreement with the assigned ν(O–O) = 898 cm^{-1} for the isolated compound in Nujol.[21] Manometry measurements indicated 1.0 ± 0.2 moles of O_2 were consumed per mole of **Ni_{isc}**. In the presence of added CN^tBu (0.4 M), the ratio was somewhat lower and increased as a function of time from 0.6 ± 0.1 to 0.8 ± 0.2.

Spectrophotometric Determination of Rates:

Bimolecular rate constants for O_2 binding (k_{O2}) were determined under pseudo first order conditions (0.05-0.35mM reduced metal compound and >10-fold excess of O_2). Reactions of **Ir**, **Ir_{dppe}** and **Pt** were studied using a conventional UV-Vis spectrophotometer equipped with a temperature control unit. Reactions were initiated by the injection of reduced metal compound into a resealable 1cm pathlength quartz cell. The headspace above the solutions was kept to a minimum in order to avoid changes in dissolved [O_2] on the timescale of experiments. Rapid kinetics measurements on **Pt, Pd, Ni** and **Ni_{isc}** were performed using an OLIS RSM 1000 equipped with a 1 cm pathlength observation cell and controlled temperature bath. Experiments were performed by rapidly mixing an N_2-saturated solution of the reduced metal compound in one drive syringe with mixtures of O_2 and N_2 in a second drive syringe. In some experiments, the solution of reduced metal compounds contained excess ligand. Absorbance data were collected in multi-wavelength mode between 300-500 nm. Global analysis was performed to determine the presence of intermediates. Time traces were fitted to a single exponential decay with background correction. The following results were analyzed to obtain k_{O2}:

Figure S1. Overlaid spectral changes for the reaction of $\mathbf{Ir_{dppe}}$ with excess O_2 in DMF at 25 °C.

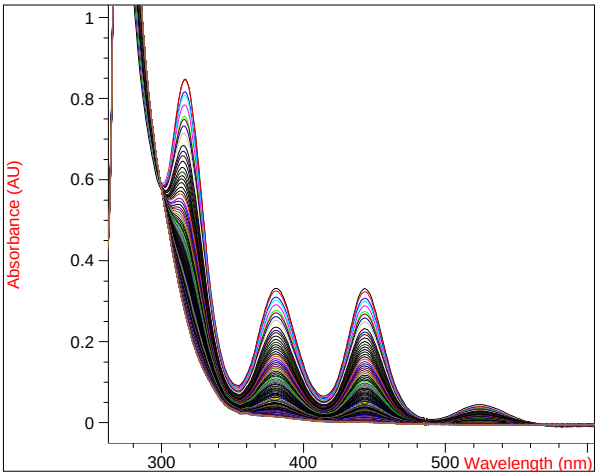

Figure S2. First order plot for the reaction of $\mathbf{Ir_{dppe}}$ with excess O_2 in DMF at 25 °C.

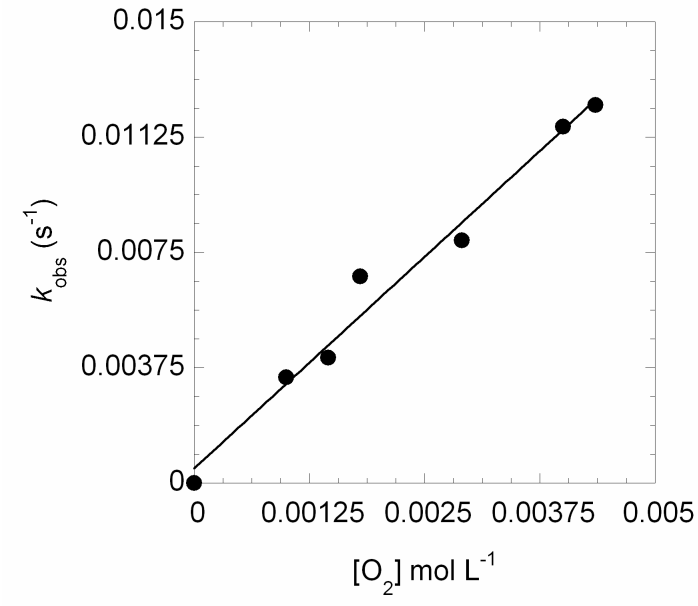

Figure S3. Overlaid spectral changes for the reaction of **Pt** with O_2 (DMF at 25 °C).

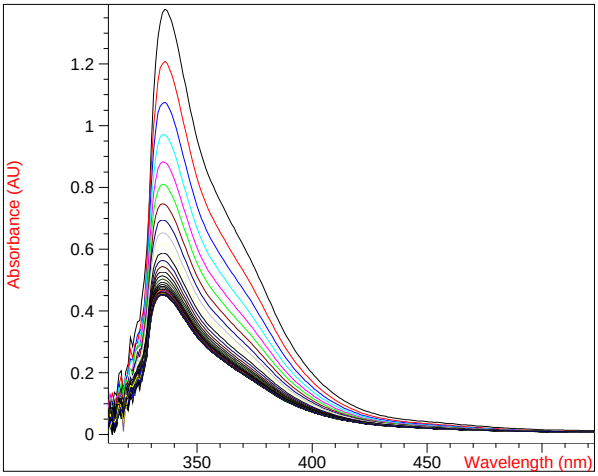

Figure S4. First order plot for the reaction of **Pt** with excess O_2 in DMF at 25 °C.

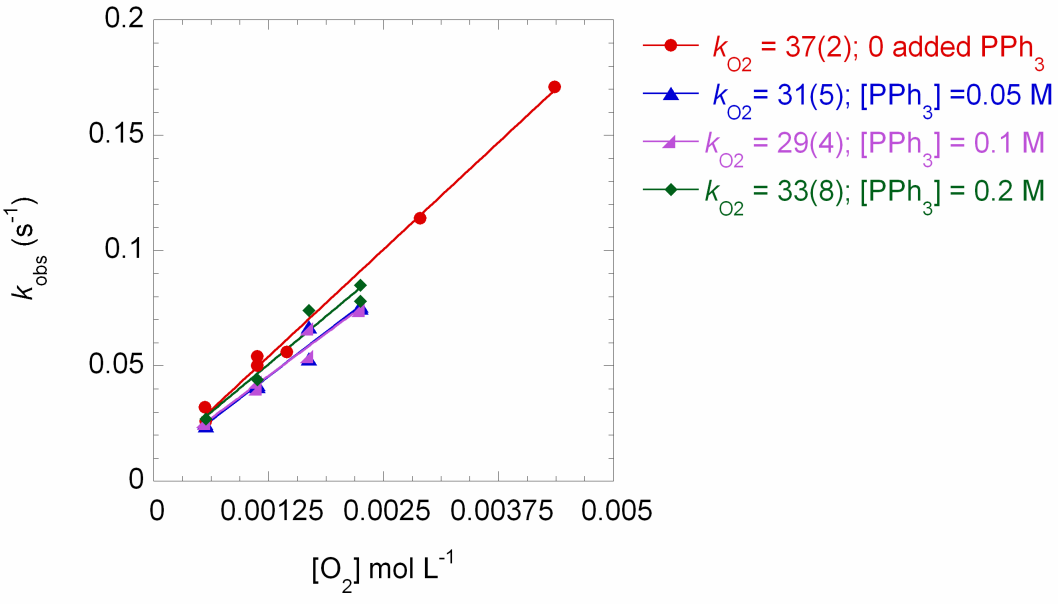

Figure S5. Optical absorbance changes for the reaction of **Pd** with O_2 (DMF at 27 °C).

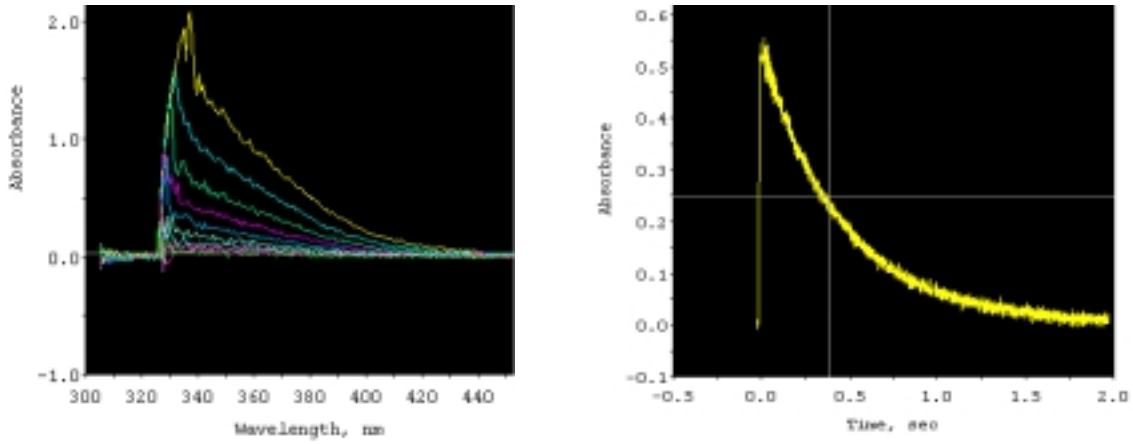

Figure S6. First order plot for the reaction of **Pd** with O_2 (DMF at 27 °C): No added PPh_3 (red circles), [PPh_3] = 0.025-0.080M (blue squares).

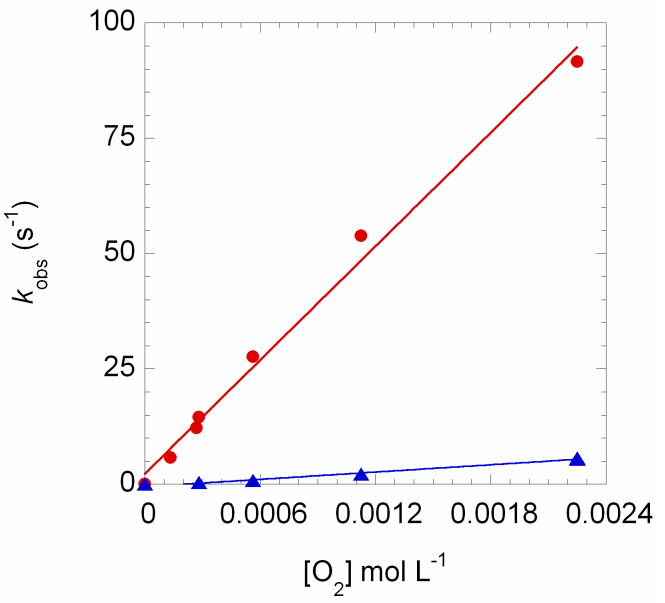

Figure S7. First order plot for the reaction of **Ni$_{isc}$** with O_2 (DMF at 27 °C) at varying concentrations of free CN^{t}Bu shown (right).

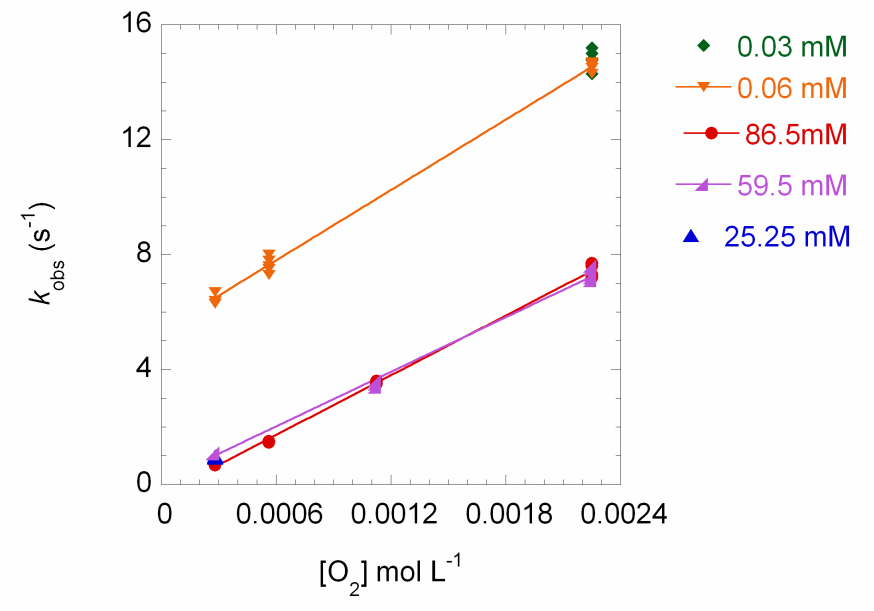

Figure S8. First order plot for the reaction of **Ni** with O_2 (DMF at 27 °C), [PPh_3] = 0.15-0.34 M.

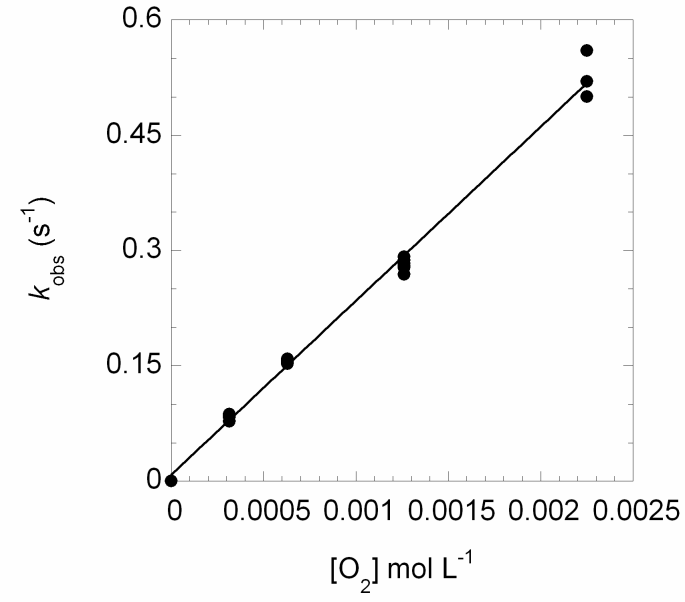

Figure S9. First order plot for the reaction of **Ni** with O_2 (DMSO at 27 °C).

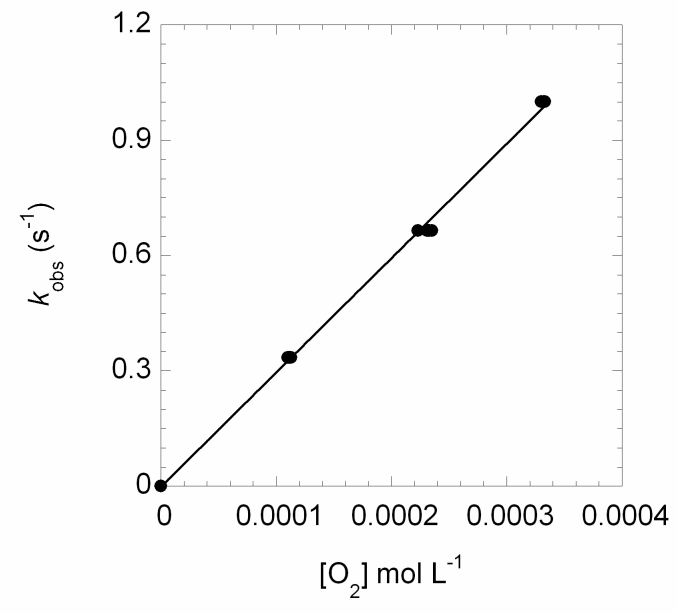

Kinetic Simulations:

KINSIM[22] was used to address reversibility of O_2 binding to Vaska's complex on the experimental time scale. The k_1 was determined directly and k_{-1} was calculated from K_{O2} = 12,000 M^{-1}. Van't Hoff analysis in DMF from 20-70 °C indicated: $\Delta G°_{298\ K}$ = -5.6 ± 0.2 kcal mol^{-1}, $\Delta H°$ = -8.4 ± 1.1 kcal mol^{-1}, $\Delta S°$ = -9.3 ± 3.3 cal $mol^{-1}K^{-1}$. Approach to equilibrium was modeled with and without contributions from the reverse reaction at $[\mathbf{Ir}]_{initial}$ = 0.25 × 10^{-3} M and 1.0 × 10^{-3} M and $[O_2]_{initial}$ = 1.0 × 10^{-3} M. **Figures S10** and **S11** demonstrate that **IrO_2** dissociation is negligible on the time scale of isotope effect measurements (up to 3 hours) consistent with the observations: (i) ^{18}k is independent of time and (ii) O_2 release is not detectable when solutions of **IrO_2** are sparged with He under dynamic vacuum at 20 °C.

(S1) $$IrCl(PPh_3)_2(CO) + O_2 \underset{k_{-1} = 1.4 \times 10^{-5}\ s^{-1}}{\overset{k_1 = 1.7 \times 10^{-1}\ M^{-1}s^{-1}}{\rightleftharpoons}} IrO_2Cl(PPh_3)_2(CO)$$

Figure S10. O_2 disappearance rates: $[\mathbf{Ir}]_i = 2.5 \times 10^{-4}$ M, $[O_2]_i = 1.0 \times 10^{-3}$ M and $[\mathbf{IrO_2}]_i = 0$.

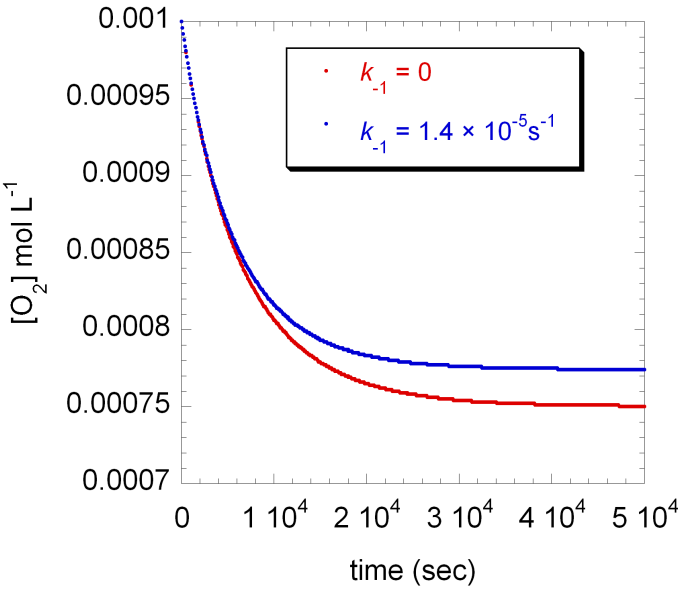

Figure S11. O_2 disappearance rates: $[\mathbf{Ir}]_i = 1.0 \times 10^{-3}$ M, $[O_2]_i = 1.0 \times 10^{-3}$ M and $[\mathbf{IrO_2}]_i = 0$.

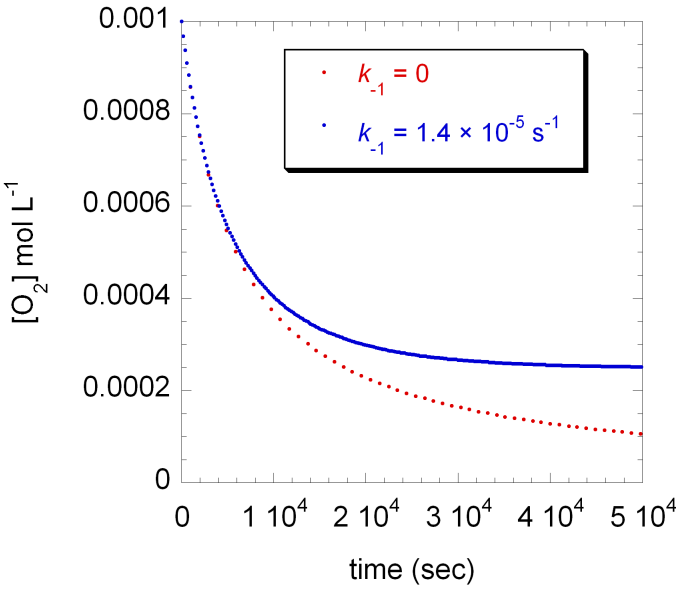

Isotope Effect Measurements:

Oxygen (^{18}O) kinetic isotope effects (^{18}k) were determined competitively following a published procedure.[23, 24] Slight modifications included the use of an injectable and collapsible gas-sampling bag[25] as the reaction vessel and a capacitance manometer with digitized readout for accurate pressure measurements. The O_2 remaining in solution after introduction of sub-stoichiometric metal compound was isolated and converted to CO_2. This is a standard procedure that facilitates sample handling. Because O_2 is completely converted to CO_2, the isotope effect on the combustion reaction does not affect ^{18}k. The pressure of CO_2 was determined and related back to the amount of O_2 consumed. The CO_2 was condensed and then flame-sealed in glass tubes for later analysis. The change in isotope ratios was fitted to Eq S2; R_0 represents the $^{18}O/^{16}O$ prior to reaction and R_f is the $^{18}O/^{16}O$ at a specific fractional consumption (f) of O_2. The ^{18}k obtained were reproducible between lots of solvent and preparations of the reduced compounds. To be as conservative as possible, errors are reported as two standard deviations about the mean calculated value.

$$^{18}k = \left[1 + \frac{\ln(R_f/R_0)}{\ln(1-f)}\right]^{-1} \quad \text{(S2)}$$

Equilibrium Isotope Effect Calculations:

Oxygen (^{18}O) equilibrium isotope effects (EIEs) were calculated for the reversible binding of natural abundance O_2 to reduced metal compounds ($^{18}K_{calc}$) using Bigeleisen's formalism and published stretching frequencies.[21, 26, 27] Experimental and calculated values for isotopically sensitive normal modes are listed in **Table 1**.

Table 1: Stretching frequencies used in ^{18}O equilibrium isotope effect calculations.[a]

	$^{16,16}\nu_{O-O}$ (cm^{-1})	$^{16,18}\nu_{O-O}$ (cm^{-1})	$^{16,16}\nu_{M-O2}$ *s* (cm^{-1})	$^{16,18}\nu_{M-O2}$ *s* (cm^{-1})	$^{16,16}\nu_{M-O2}$ *a* (cm^{-1})	$^{16,18}\nu_{M-O2}$ *a* (cm^{-1})
O_2[b]	1556.3	1512.5	—	—	—	—
IrO_2[c,d]	858	834	581	572	595	586
$Ir_{dppe}O_2$[c]	843	818	547	538	533	524
PtO_2[d]	827	804	470	460	488	478
PdO_2[e]	877	854	496	486	487	477
$Ni_{isc}O_2$[d]	897	873	560	550	523	513

[a]Metal–O stretches designated symmetric (*s*) and asymmetric (*a*). [b]Ref. 28. [c]Ref. 26. [d]Ref. 21. [e]Ref. 27.

The equilibrium isotope effect is defined according to S3 where **A** and **B** correspond to initial and final states of O_2, respectively, and the asterisk designates the site of the heavy isotope. ^{18}K is calculated using eq S4[29]with terms corresponding to mass and moments of inertia (*MMI*), excited state vibrational energies (*EXC*) and zero-point energy (*ZPE*). Equations S5-S7 define these reduced partition functions in terms of stretching frequencies (ν) and temperature (*T*); *h* is Planck's constant and *k* is Boltzmann's constant. The *MMI* term, representing translational and rotational degrees of freedom, is expressed as a running product (*VP*) according to the Redlich-Teller product rule.[30] The equations were solved using the Java swing application Equilibrium Isotope Effect Input/Output (EIE I/O). The results (**Table 2**) are based on models which treat the product as having an isosceles triangle geometry and three isotopically sensitive normal modes: ν_{O-O}, symmetric ν_{M-O2} and asymmetric ν_{M-O2}. Analogous to other associative mechanisms, a large contribution from *MMI* is observed.[30] Whether this feature reflects loss of isotope discrimination of rotational and translational modes upon binding O_2 to a heavy metal fragment will be the subject of future investigations.

(S3)

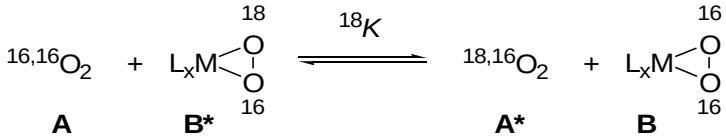

(S4) $$^{18}K = MMI \times EXC \times ZPE$$

(S5) $$MMI = VP = \frac{\prod_{j}^{3N-6}\left(\nu_j{}^{B} / \nu_j{}^{B*}\right)}{\prod_{i}^{3N-5}\left(\nu_i{}^{A} / \nu_i{}^{A*}\right)}$$

(S6) $$EXC = \frac{\left[\prod_{j}^{3N-6}\frac{1-\exp^{-\left(h\nu_j{}^{B*}/kT\right)}}{1-\exp^{-\left(h\nu_j{}^{B}/kT\right)}}\right]}{\left[\prod_{i}^{3N-5}\frac{1-\exp^{-\left(h\nu_i{}^{A*}/kT\right)}}{1-\exp^{-\left(h\nu_i{}^{A}/kT\right)}}\right]}$$

(S7) $$ZPE = \frac{\left[\prod_{j}^{3N-6}\frac{\exp^{\left(h\nu_j{}^{B*}/2kT\right)}}{\exp^{\left(h\nu_j{}^{B}/2kT\right)}}\right]}{\left[\prod_{i}^{3N-5}\frac{\exp^{\left(h\nu_i{}^{A*}/2kT\right)}}{\exp^{\left(h\nu_i{}^{A}/2kT\right)}}\right]}$$

Table 2: Partition functions and ^{18}O equilibrium isotope effects computed from calculated stretching frequencies in Table 1.

Compound	*EXC*	*ZPE*	*MMI*	^{18}K
$\mathbf{IrO_2}$	0.9926	1.0044	1.0312	1.028
$\mathbf{Ir_{dppe}O_2}$	0.9909	1.0019	1.0358	1.028
$\mathbf{PtO_2}$	0.9871	1.0019	1.0428	1.031
$\mathbf{PdO_2}$	0.9883	1.0019	1.0399	1.030
$\mathbf{Ni_{isc}O_2}$	0.9907	0.9995	1.0365	1.026

References

[1] W. Armarego, C. Chai, *Purification of Laboratory Chemicals*, Butterworth-Heinemann, Amsterdam, **2003**.

[2] J. P. Collman, C. T. Sears, Jr., M. Kubota, *Inorg. Synth.* **1990**, *28*, 92.

[3] K. D. Schramm, T. H. Tulip, J. A. Ibers, *Inorg. Chem.* **1980**, *19*, 3183.

[4] R. A. Vanderpool, H. B. Abrahamson, *Inorg. Chem.* **1985**, *24*, 2985.

[5] R. Brady, B. R. Flynn, G. L. Geoffroy, H. B. Gray, J. Peone, Jr., L. Vaska, *Inorg. Chem.* **1976**, *15*, 1485.

[6] L. Vaska, D. L. Catone, *J. Am. Chem. Soc.* **1966**, *88*, 5324.

[7] G. L. Geoffroy, M. S. Wrighton, G. S. Hammond, H. B. Gray, *J. Am. Chem. Soc.* **1974**, *96*, 3105.

[8] R. Ugo, F. Cariati, G. La Monica, *Inorg. Synth.* **1968**, *11*, 105.

[9] A. Sen, J. Halpern, *Inorg. Chem.* **1980**, *19*, 1073.

[10] J. P. Birk, J. Halpern, A. L. Pickard, *J. Am. Chem. Soc.* **1968**, *90*, 4491.

[11] A. Sen, J. Halpern, *J. Am. Chem. Soc.* **1977**, *99*, 8337.

[12] L. Malatesta, M. Angoletta, *J. Chem. Soc.* **1957**, 1186.

[13] C. A. Tolman, W. C. Seidel, D. H. Gerlach, *J. Am. Chem. Soc.* **1972**, *94*, 2669.

[14] N. W. Aboelella, J. T. York, A. M. Reynolds, K. Fujita, C. R. Kinsinger, C. J. Cramer, C. G. Riordan, W. B. Tolman, *J. Chem. Soc., Chem. Commun.* **2004**, 1716.

[15] S. D. Ittel, *Inorg. Synth.* **1990**, *28*, 98.

[16] R. Mynott, A. Mollbach, G. Wilke, *J. Organomet. Chem.* **1980**, *199*, 107.

[17] G. Bontempelli, F. Magno, B. Corain, G. Schiavon, *J. Electroanal. Chem. Interfacial Electrochem.* **1979**, *103*, 243.

[18] S. Thomas, W. L. Reynolds, *J. Chem. Phys.* **1967**, *46*, 4164.

[19] S. Otsuka, A. Nakamura, Y. Tatsuno, *J. Am. Chem. Soc.* **1969**, *91*, 6994.

[20] S. Otsuka, T. Yoshida, Y. Tatsuno, *J. Am. Chem. Soc.* **1971**, *93*, 6462.

[21] A. Nakamura, Y. Tatsuno, M. Yamamoto, S. Otsuka, *J. Am. Chem. Soc.* **1971**, *93*, 6052.

[22] B. A. Barshop, R. F. Wrenn, C. Frieden, *Anal. Biochem.* **1983**, *130*, 134.

[23] J. P. Roth, J. P. Klinman, in *Isotope Effects in Chemistry and Biology* (Eds.: A. Kohen, H. Limbach), CRC Press, Boca Raton, **2005 in press**.

[24] G. Tian, J. A. Berry, J. P. Klinman, *Biochemistry* **1994**, *33*, 226.

[25] Tedlar © gas samples bags were supplied by the MiDan Co. (Chino, CA).

[26] R. W. Horn, E. Weissberger, J. P. Collman, *Inorg. Chem.* **1970**, *9*, 2367.

[27] P. J. Hayward, D. M. Blake, G. Wilkinson, C. J. Nyman, *J. Am. Chem. Soc.* **1970**, *92*, 5873.

[28] G. Tian, J. P. Klinman, *J. Am. Chem. Soc.* **1993**, *115*, 8891.

[29] J. Bigeleisen, M. Goeppert-Mayer, *J. Chem. Phys.* **1947**, *15*, 261.

[30] W. P. Huskey, in *Enzyme Mechanism from Isotope Effects* (Ed.: P. F. Cook), CRC Press, Boca Raton, **1991**.